

## 2 m survey method and its improved device application in Dongshan geothermal field in Xiamen in China

YanJun Zhang<sup>1,2</sup> · Yangyang Xie<sup>1</sup>  · Tong Zhang<sup>1</sup> · Tong Liu<sup>1</sup> · Chi Zhang<sup>1</sup>

Received: 30 May 2016 / Accepted: 3 September 2016 / Published online: 23 September 2016  
© Springer-Verlag Berlin Heidelberg 2016

**Abstract** Preliminary geothermal surveys to identify areas of potential geothermal anomalies are the most important stage in traditional hydrothermal-type geothermal resource exploration procedures. Temperature gradient wells are limited because of their accessibility issues and high costs, whereas the 2 m survey is considered a rapid, efficient, and inexpensive method to measure temperature accurately and allow for rapid vectoring toward geothermal anomalies in cases where thermal groundwater is not overlain by near-surface cold aquifers. An improved quick and portable measurement device is developed that adds in situ thermal conductivity tests based on temperature. The device, which is easy to assemble, portable, and suitable for two or three people in field work, had been calibrated by laboratory experiments. The device was applied in Dongshan geothermal field, Xiamen City in China, and 18 measurement positions were arranged. Results clearly described the geothermal anomalies in the area and revealed two temperature anomaly centers, namely a strong one in the eastern area and a weak one in the western area. Moreover, a speculated fault provided a hydraulic connection between the eastern and western areas. According to the 2 m survey, a steady-state heat conduction model has

been used to inverse the 20 m temperature. The average temperature error of all boreholes in 20 m is 3 °C, whereas the relative errors between actual and forecast values are less than 10 %. Therefore, the 2 m survey method and improved device shows good performance in preliminary geothermal surveys.

**Keywords** Shallow measurement · Geothermal survey · Thermal conductivity · Dongshan

### Introduction

Geothermal energy is a competitive type of clean renewable energy. A hydrothermal-type geothermal resource refers to geothermal energy with high-temperature fluid hosted in high-permeability pores or fractures (Wang et al. 2012). Traditional hydrothermal-type geothermal resource exploration procedures usually include the following stages: (1) the preliminary survey stage, where surface anomalies are investigated (including hot springs, fumaroles, and salt tufa), after which geothermal areas are identified by comprehensive judgment of small-scale geological data and remote sensing data. (2) The geophysical and geochemical exploration stages, where magnetotelluric and controlled source audiomagnetotellurics or other methods are used in potential areas to continue to narrow the scope and determine the drilling positions (Kana et al. 2015). (3) The drilling survey stage, where temperature gradient wells are drilled to verify whether geothermal reservoirs exist. Generally, as each stage progresses, the economic cost will correspondingly increase to a higher level, particularly in the drilling stage, which requires a substantial cost but obtains limited temperature data by restricted boreholes (Zehner et al. 2012). The preliminary

---

This article is part of a Topical Collection in Environmental Earth Sciences on “Subsurface Energy Storage II”, guest edited by Zhonghe Pang, Yanlong Kong, Haibing Shao, and Olaf Kolditz.

---

✉ Yangyang Xie  
935036922@qq.com

<sup>1</sup> College of Construction Engineering, Jilin University, Changchun 130026, China

<sup>2</sup> Key Lab of Groundwater Resource and Environment, Ministry of Education, Jilin University, Changchun 130026, China

survey stage is the most important but is also the most challenging. During the preliminary stage, drilling is still the current most accurate method of identifying a potential geothermal anomaly area (Aretouyap et al. 2016). Although this method can accurately obtain the temperature data of the underground soil in target depth, its high costs limit its frequency of application. Thus, delineating geothermal anomaly areas may not match actual conditions because of the lack of underground temperature data during the preliminary survey stage.

Shallow temperature measurement is a method of measuring shallow-depth ground temperatures to identify geothermal anomaly areas. Compared with traditional methods, shallow temperature measurement is cheaper, more effective and can obtain substantial temperature data in a short period of time. Temperature measurements can be divided into three main categories (Sladek et al. 2007) depending on the depth below the surface at which the temperatures are measured, as follows: (1) surface measurements, (2) measurements at depths of 0–20 m, and (3) measurements at depths >20 m. Surface temperatures are easiest to obtain but are strongly affected by environmental factors and thus cannot identify geothermal heat contributions. Temperatures at depths of 0–20 m are affected by daily and seasonal temperature cycles on the earth's surface (Coolbaugh et al. 2007), but the influence of daily and seasonal temperature cycles decreases with the increase in depth at which temperature measurements are taken. Temperatures at depths >20 m are largely unaffected by daily and seasonal (annual) solar radiation and climate change (LeSchack and Lewis 1983). Although 20 m temperature data can be obtained by drilling, the time and cost are severely limited. At a depth of 1 m, temperature variations induced by the 24-h solar radiation cycle are almost completely damped out (Elachi 1987). Temperature distributions in shallow areas have been analyzed by environmental influences (Kappelmeyer 1957). The 1 m temperature was used to identify the distribution of geothermal hot springs (Sugawa 1961). Based on the 1 m temperature surveys, underground hot springs are speculated by the variations in ground temperature distribution (Urakami 1968). According to this method, shallow temperature differences between underwater reservoirs and discharge areas were investigated so that the underground water flow paths could be inferred (Cartwright 1974). The shallow measurement method was first used to depict the geothermal anomaly at the preliminary survey stage in Nevada (Olmsted 1977). Several 1 m surveys have been successfully conducted at various locations in the Great Basin (Trexler et al. 1982a, b). In 2007, the shallow measurement method was significantly improved by Great Basin

Center for Geothermal Energy and University of Nevada and the 2 m survey method was first proposed (Coolbaugh et al. 2007). Compared with traditional 1 m survey method, 2 m survey method, which is a new shallow measurement method, performs better in reducing environmental impact and reflects more real geothermal anomaly. Several geothermal fields (including Dead Horse Wells, Hawthorne Army Depot, and Terraced Hills) were successfully predicted and detected by this novel method. (Kratt et al. 2010). Compared with the early-stage geothermal survey efficiency of Geoprobe and Drilling, the 2 m survey was shown to be a good technique to identify and delineate geothermal outflow zones prior to more expensive temperature gradient drilling (Zehner et al. 2012).

Shallow temperature measurements have not been more widely used in geothermal exploration in the past because they are usually time-consuming and not fully field-portable (Coolbaugh et al. 2007). The traditional measurement equipment was limited to vehicles, and the temperature sensors were separated by metal rods in soil to eliminate frictional interference; thus, the measurement would last for 1 h at every measurement position (Sladek et al. 2007). Although the 2 m survey method has been well applied for a few years, recent research on improving it has been relatively rare. The main objectives of this work are as follows: (1) to develop an improved quick and portable measurement device that reduces survey time and is independent of vehicles; (2) to add in situ thermal conductivity tests based on temperature tests which calibrated by laboratory experiment to improve the accuracy of the 2 m method at the early survey stage; and (3) to enhance survey accuracy of geothermal area identification. This study will use this improved survey device in Xiamen City in China and combine an in situ thermal conductivity analysis with a temperature inverse forecast to increase preliminary geothermal survey accuracy and provide survey experience for other similar potential geothermal fields in China.

## Testing equipment

### Device structure design

#### *Boring device*

The boring device comprises a walk-behind power plant, drill pipes, and a drill bit (Fig. 1). The walk-behind power plant consists of a small gasoline engine (1E48F) made by HuaSheng<sup>®</sup> with dimensions of 285 mm × 195 mm × 282 mm. The gasoline engine possesses a large torque and a low speed, and its maximum power is 2.2 kW with a

speed of 7500 r/min. The drill pipes are made of hardened steel and were designed to use a hollow tube with an average length of 120 cm and a diameter of 10 mm in each pipe. Two pairs of nail holes are designed in both sides of the drill pipe to allow convenient connection with the walk-behind power plant or the next pipe. The auger drill bit is selected for its efficient drilling capability. The drill bit is made of a hard alloy to ensure that it can drill in most conditions. The boring device can be dismantled, stored in a suitcase, and easily transported.

*Measuring probe*

A large length-to-diameter ratio is designed for the probe to keep the soil samples in the unbounded heat-conducting media relative to the probe and to avoid axial heat conduction. Thus, the diameter of the probe is 2 mm and the

length of the probe is 200 mm. The probe is designed in a small volume so that the thin but long probe can be easily inserted into the ground. In this case, the insertion procedure causes limited influence on the underground temperature field. The probe is composed of a needle tip, a stainless steel seamless slimline pipe, and a pin cap (Fig. 2).

The needle tip is made of hard alloy that can reach the bottom of bores in most conditions. The stainless steel seamless slimline pipe is used to seal the temperature sensor and heating wire. The resistance temperature detector (RTD) is selected as the temperature sensor. The sensor consists of a PT1000 resistance temperature sensor (precision = 1/3 DIN Class B, temperature error =  $\pm(0.10 + 0.0017|t|)$ , TCR = 3850 ppm/°C), which has a precision of 0.1 °C. The heating wire is made of enameled Constantan wire (resistance = 62.28 Ω/m, TCR =  $40 \times 10^{-6}$  ppm/°C), which is small, has high resistance, and shows minimal change of resistivity with temperature variety. By contrast, the enameled wire also possesses features of insulation, antioxidation, and thermostabilization. The pin cap on top of the stainless steel seamless slimline pipe is used to fix the probe. The probe is connected with a long silver wire through the hole on the tail of the pin cap to allow data transmission to the receiving device at the surface.

Placing the pin caps, which are the most fragile part of the measurement test, on top of the probe is advisable. Thus, the probe can be maintained or replaced easily should corrosion or damage occur.

*Data receiving device*

The temperature acquisition microcontroller is a 16-bit MCU (MSP430F5438) made by Texas Instruments® (TI®). The I–V conversion circuit is designed to transform the PT1000 resistance variation into temperature data for storage in the programmable logic controller (PLC). The analog-to-digital converter (ADC) is ADS1240, which was also made by TI®. The measurement circuit is made by REF50xx. A battery is used to supply the power for the MCU, PLC, ADC and measurement circuit. The entire receiving device is sealed in a small electrical panel box

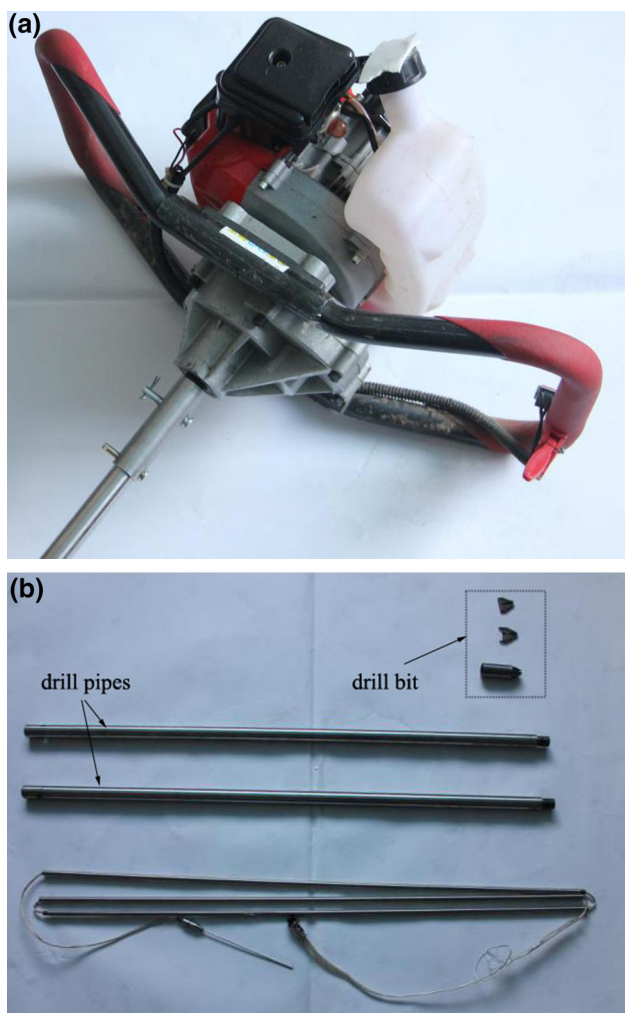


**Fig. 1** The boring device comprises three parts, including a walk-behind power plant, drill pipes, and a drill bit. **a** The walk-behind power plant is made of a small gasoline engine. **b** In the design, drill pipes use a hollow tube, and the drill bit can be detached

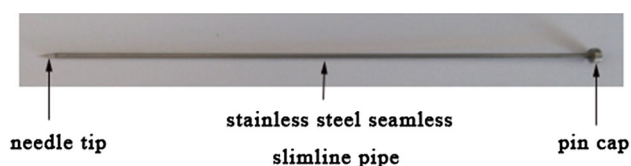


**Fig. 2** The 200-mm-long measure probe exhibits a diameter of 2 mm. It features three basic components, namely a needle tip, a stainless steel seamless slimline pipe, and a pin cap

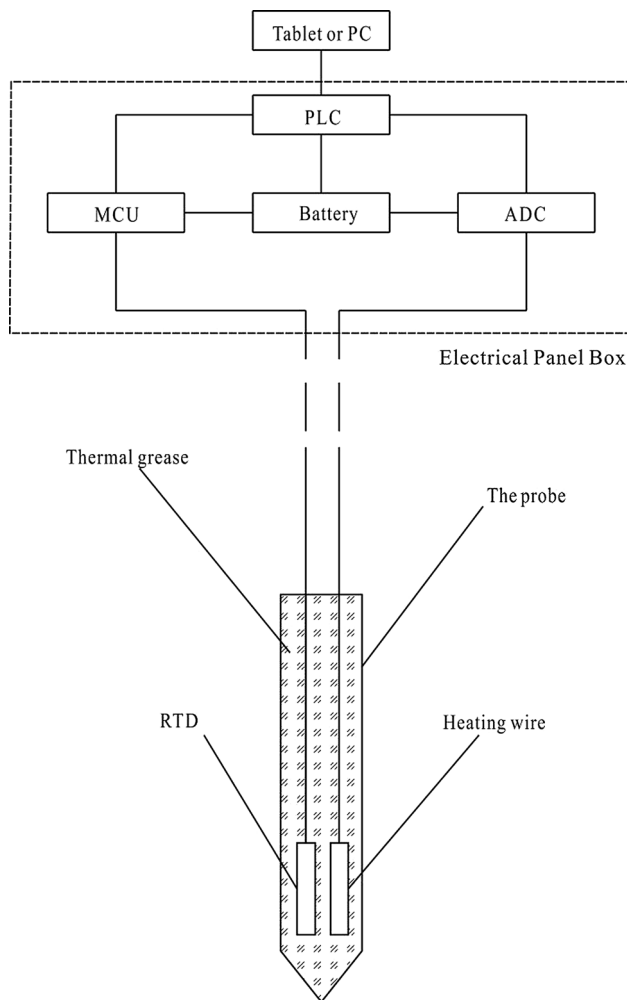


**Fig. 3** Design patterns of the data receiving device

(Fig. 3). A software we composed by C# is used to process the data. The original data can be logged in the PLC and then introduced into the software in a tablet or PC. The data receiving device can be controlled by keyboard and touch screen. However, the software can only be run on Microsoft Windows.

**Operation introduction**

The boring device should be assembled before the test. One side of the drill pipe is linked to the auger drill, and the other side of the drill pipe connects the walk-behind power plant with the joint by nails. Thus, the drill pipe screws will not be excessively tight, and the contraction can be easily disassembled for connection with the succeeding pipe. We begin drilling the borehole until the drill pipe is completely drilled into the ground. Then, we remove the walk-behind power plant, link it to the succeeding pipe, and continue the process. The borehole is completed when the drill bit reaches the target depth. Finally, we connect the measuring

probe with the data receiving device. The probe is inserted into the target depth through the hollow drill pipes to avoid borehole collapse and to minimize the amount of thermal disturbance caused by drilling. After the probe is inserted into undisturbed soil at the bottom of the borehole by its needle tip, we open the measurement circuit and begin the test.

**Measurement theoretical basis**

The needle probe method was first used to measure thermal conductivity (Von Herzen and Maxwell 1959). Numerous experiments have used this method (Rao and Singh 1998; Manthena and Singh 2001). The heat source model is based on unsteady heat conduction in unbounded media (Popov et al. 2012). Assuming that the underground soil mass is an unbounded heat-conducting media relative to the probe, the initial temperature of the layer is stable and the thermal parameters are constant as soil temperature fluctuates. The probe can be regarded as a line heat source. Heat conduction is a one-dimensional axisymmetric problem around the probe. According to the above assumptions, the distribution function of surplus temperature fields can be deduced from primitive equations (Carslaw and Jaeger 1959) and simplified as follows:

$$\theta = t - t_0 = \frac{-q}{4\pi\lambda} E_i \left[ -\frac{r^2}{4\alpha\tau} \right] \tag{1}$$

where  $\theta$  is the surplus temperature;  $t$  is the temperature at time  $\tau$ ;  $t_0$  is the initial temperature;  $q$  is the heating power;  $\lambda$  is the soil thermal conductivity;  $E_i$  is the exponential integral function;  $r$  is the distance between a point and line heat source;  $\alpha$  is the thermal diffusivity; and  $\tau$  is the heating time. When  $r$  is sufficiently small and  $\tau$  is sufficiently large,  $E_i$  can be calculated as follows:

$$E_i(-\mu) = C + \ln(\mu) \tag{2}$$

where  $\mu = r^2/4\alpha\tau$ ;  $C$  is Euler’s constant, whose value is 0.57726.

Equation (2) is substituted into Eq. (1):

$$\theta = t - t_0 = \frac{-q}{4\pi\lambda} \left[ -C - \ln \frac{r^2}{4\alpha\tau} \right] \tag{3}$$

By calculating Eq. (3), the temperature of  $r$  can be written as follows:

$$\theta_2 - \theta_1 = t_2 - t_1 = \frac{q}{4\pi\lambda} \ln \frac{\tau_2}{\tau_1} \tag{4}$$

Equation (4) can be rewritten as follows:

$$\frac{4\pi\lambda}{q} = \frac{\ln \tau_2 - \ln \tau_1}{t_2 - t_1} \tag{5}$$

Equation (5) shows that  $\ln \tau$  and  $t$  possess a linear relationship. The curve of  $\ln \tau$  and  $t$  can be obtained by the least squares method. The relationship of  $\ln \tau$  and  $t$  can be defined as follows:

$$\ln \tau = \alpha_0 + \alpha_1 t \tag{6}$$

The sum of the deviation squares of  $\ln t_i$  and  $\ln \tau_i$  can be considered an optimal criterion. Thus,  $\alpha_0$  and  $\alpha_1$  can be calculated as follows:

$$\alpha_0 = \frac{\sum \ln \tau_i - \alpha_1 \sum t_i}{n} \tag{7}$$

$$\alpha_1 = \frac{n \sum t_i \ln \tau_i - \sum t_i \sum \ln \tau_i}{n \sum t_i^2 - (\sum t_i)^2} \tag{8}$$

The soil thermal conductivities ( $\lambda_i$ ) can be calculated as follows:

$$\lambda_i = \frac{q}{4\pi} \frac{n \sum t_i \ln \tau_i - \sum t_i \sum \tau_i}{n \sum t_i^2 - (\sum t_i)^2} \tag{9}$$

Based on the previously presented principles, the temperature of the soil sample can be measured immediately after the probe is inserted into the soil. When the thermal conductivity is measured, the measurement circuit opens and the heating wire and the temperature sensor begin to work. Timing when  $\tau = 0$ , and the time of temperature collection is recorded. The thermal conductivity ( $\lambda_i$ ) at time  $\tau_i$  is calculated by using Eq. (9). The tablet or computer can display the variation curves of the thermal conductivity of soil.

### Calibration of the equipment

The improved device was tested in a laboratory before being used in the field. Another controlled test was used as a comparison. The control group was tested by QTM (Showa Denko®), which is a typical thermal conductivity equipment in laboratory experiments. The QTM uses an unsteady method that is the basis of the hot strip method. Comparisons of the two method (Zhang et al. 2009) results are used to validate the precision and calibration of the improved device.

### Preparation of the soil samples

In the laboratory experiment, the tests were applied in three kinds of soil samples, namely coarse sand, fine sand, and silty clay. The three remolded samples were tested in varying levels of water content. At the beginning, the soil samples were dried to constant weight in a vacuum oven. Then, the dehydrated samples were saturated by adding distilled water with 2–5 % of the gradient until the samples were saturated.

The length of the probe must be considered when we rebuild the soil sample boxes. Based on the needle probe method, the probe had to be inserted at the center of the soil samples. For this purpose, a small round hole was supposed to be punched at the center on one side of the soil sample box with a sufficiently long diameter to locate the probe. By contrast, the size of the soil sample for QTM had to be at least 150 mm × 60 mm × 20 mm in length, width, and thickness, respectively. The soil samples were designed in the size of 150 mm × 60 mm × 60 mm to meet the aforementioned requirements.

### Laboratory experiment

The measuring probe and QTM are used to measure every soil sample to verify the results of thermal conductivity obtained by the measuring probe. Temperature sensors placed around the soil sample box showed that the heat emitted by the probe would not affect the edge of soil samples. Thus, the soil samples are unbounded heat-conducting media relative to the probe. The measuring probe was inserted into the middle of the soil sample and heated with different work voltages for the same sample. Regardless of the voltage applied, the heating time was fixed at 150 s.

The tendency of thermal conductivity to vary among soil samples can be observed clearly based on the relationship between soil thermal conductivity and heating time depicted in Fig. 4. The soil thermal conductivity surged drastically at the beginning, but as the heating time elapsed, the degree of the variation decreased gradually. Eventually, the variation of soil thermal conductivity

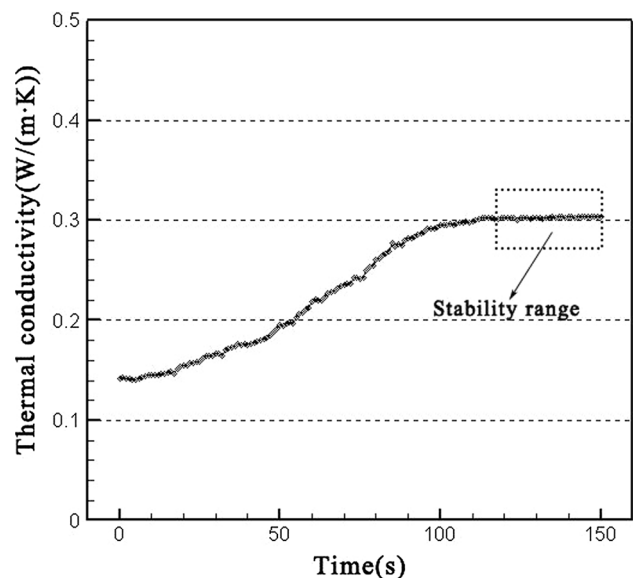


Fig. 4 Thermal conductivity of coarse sand sample with 2 % water content measured by probe in 9 V work voltage

almost stopped. When the variation tendency was stable, the result of soil thermal conductivity was considered close to the real value. Thus, the final result was selected based on the time for which the thermal conductivity remained stable and was calculated by the least squares method. Each soil sample was measured five times, and the average value was used as the value of the thermal conductivity of the soil samples by both devices.

### Result comparison

No failure data appeared according to the measurement report of soil samples in different water contents. The detailed results are shown in Table 1.

The thermal conductivity of coarse sand varied from 0.232 W/(m K) to 2.291 W/(m K) and the thermal conductivity of fine sand varied from 0.196 W/(m K) to 1.493 W/(m K) and the thermal conductivity of silty clay varied from 0.211 W/(m K) to 1.573 W/(m K). The probe measuring range satisfies the general requirements of soil thermal conductivity. The variety of thermal conductivity could be stabilized after no more than 150 s of heating time for every sample. When the heating voltage was increased gradually, the stable temperature of the sensor inserted into the soil sample increased and the setting time was prolonged. Furthermore, thermal conductivity also increased gradually for the same sample. Increases in water content increased soil thermal conductivity to varying degrees. The soil thermal conductivity increased significantly when the water content was low and was basically stable when the soil samples were saturated.

According to Table 1, when the water content was below threshold, which represented specific water contents in different samples, the thermal conductivity estimated by the measuring probe was generally smaller than the result obtained by the QTM. As the water content increased gradually until it surpassed the threshold, the thermal conductivity measured by the probe surpasses the QTM fluctuated up and down. A 3 V work voltage was too low to provide sufficient power for heating; thus, the temperature increased inconspicuously and led to the thermal conductivity remaining smaller than the QTM. Compared with the QTM results, in low water content (<8 %), the thermal conductivity deviations measured at 6 V were smaller by 3.2 %, whereas those measured at 9 V were smaller by 2.0 % than the results obtained by the QTM. With the increase in water content, the deviations for samples heated with 6 V work voltage were smaller by 0.5 % on average, whereas the deviation for samples heated with 9 V work voltage was larger by 1.6 % on average. Therefore, the final measuring probe work voltage was calibrated by 10 V in low water content and 7.5 V in the saturated condition. The average calibrated deviations in both voltages are less than 2 % in Table 2.

## Field experiment in Xiamen City

### Study area

Xiamen City is located in the southeastern area of Fujian Province in China and lies 1.5° north of the Tropic of Cancer, which possesses a marine monsoon climate with abundant precipitation and sunshine. The field experiment area in Dongshan is located northeast of Xiamen City (Fig. 5).

The annual average temperature of Dongshan is 21 °C with no evident division among the four seasons. The surface terrain of Dongshan is gentle, and its geographical feature is simple. The land is mainly covered by alluvial soil and diluvium soil during the Quaternary Period. The water table of the field experiment area is high, and its depth ranges from 0.3 to 5 m. Several underwater spring spots are observed in the eastern and western areas of Dongshan. Spring artesian can be observed, and the highest water temperature is approximately 38.6 °C (Fig. 6).

The field survey data are collected by the Geological Engineering Investigation Institute of Xiamen City. Monitoring wells and measurement wells are drilled to obtain a general idea of the location of geothermal anomalies and the temperature details in shallow underground. Areas with geothermal anomalies exhibit an elliptical or irregular circle loop shape. Two high-temperature thermal centers are detected in the anomaly area. A large effect range has been influenced by one thermal anomaly center where the maximum temperature is 70.3 °C at a depth of 20 m. The other anomaly center only measured approximately 45 °C at a depth of 20 m and played a role in a smaller range.

### Experimental design

The potential geothermal anomaly area covers an area of approximately 1 km<sup>2</sup>, and two spring spots are traced. Based on the experience of shallow (1–2 m) temperature measurements in New Zealand (Thompson 1964), 18 measurement positions are arranged divergent in distance according to the two spring spots in the potential geothermal anomaly area (Fig. 7).

The measurement positions are adjusted properly to avoid the ponds or surface runoff areas. The shallow soil is mainly covered by clay. The boring device is used to drill the borehole, and the probe is inserted into the hollow drill pipes to the target depth. Although most of the measurement positions are water-saturated or approximately water-saturated, the influence of measurement is limited because of the low permeability of

**Table 1** Thermal conductivity result of soil samples estimated by both QTM and measure probe

No	Sample code	Water content (%)	QTM (W/m K)	Measure probe (3 V)			Measure probe (6 V)			Measure probe (9 V)		
				Thermal conductivity (W/m K)	Temperature vary (°C)	Stable time (s)	Thermal conductivity (W/m K)	Temperature vary (°C)	Stable time (s)	Thermal conductivity (W/m K)	Temperature vary (°C)	Stable time (s)
1	CS00	0	0.282	0.232	4	60	0.255	8	82	0.273	15	104
2	CS02	2	0.315	0.284	3	60	0.293	8	90	0.303	13	118
3	CS04	4	0.398	0.35	1.5	63	0.362	5	80	0.37	9	95
4	CS06	6	0.858	0.815	3	65	0.828	6	85	0.849	11	105
5	CS08	8	1.047	0.91	4	75	1.045	7	95	1.105	14	120
6	CS10	10	1.528	1.484	3.5	70	1.581	8	90	1.612	15	115
7	CS12	12	2.052	1.85	4	75	1.988	8.5	95	2.042	14	125
8	CS16	16	2.263	2.23	4	76	2.313	7	80	2.291	13	120
9	XS00	0	0.216	0.196	3	65	0.198	7	95	0.201	13	100
10	XS02	2	0.226	0.204	2.2	60	0.207	8	100	0.211	14	120
11	XS04	4	0.34	0.339	3.5	70	0.358	8	90	0.342	12	115
12	XS06	6	0.533	0.542	4	68	0.544	8.5	96	0.547	11.5	110
13	XS08	8	0.65	0.643	4	70	0.654	9	112	0.668	12	124
14	XS10	10	0.755	0.69	3	72	0.723	9.3	110	0.75	10	110
15	XS13	13	0.858	0.813	3.5	78	0.832	9.5	115	0.897	14	120
16	XS16	16	1.136	1.075	3	65	1.135	8.8	95	1.178	13	125
17	XS20	20	1.365	1.342	4	70	1.381	9	90	1.401	12	115
18	XS25	25	1.47	1.412	3	65	1.456	7	98	1.493	13	120
19	FT00	0	0.216	0.211	3	65	0.215	7	90	0.215	12	120
20	FT03	3	0.281	0.274	3	72	0.274	8	97	0.283	13	115
21	FT07	7	0.435	0.443	4	78	0.434	8.5	95	0.432	12	125
22	FT11	11	0.835	0.835	3.5	70	0.854	8	90	0.837	11	120
23	FT15	15	1.254	1.243	4	70	1.245	7.5	100	1.265	12	124
24	FT20	20	1.365	1.335	3	65	1.353	7	96	1.37	13	120
25	FT25	25	1.57	1.495	3.5	70	1.535	8	100	1.573	12	125

**Table 2** Thermal conductivities of soil samples measured by calibrated voltage

No	Sample code	Water content (%)	QTM (W/m K)	Measure probe (7.5 V) Thermal conductivity (W/m K)	Measure probe (10 V) Thermal conductivity (W/m K)
1	CS04	4	0.398	–	0.381
2	XS04	4	0.34	–	0.348
3	FT03	3	0.281	–	0.288
4	CS16	16	2.263	2.277	–
5	XS25	25	1.47	1.463	–
6	FT25	25	1.57	1.545	–

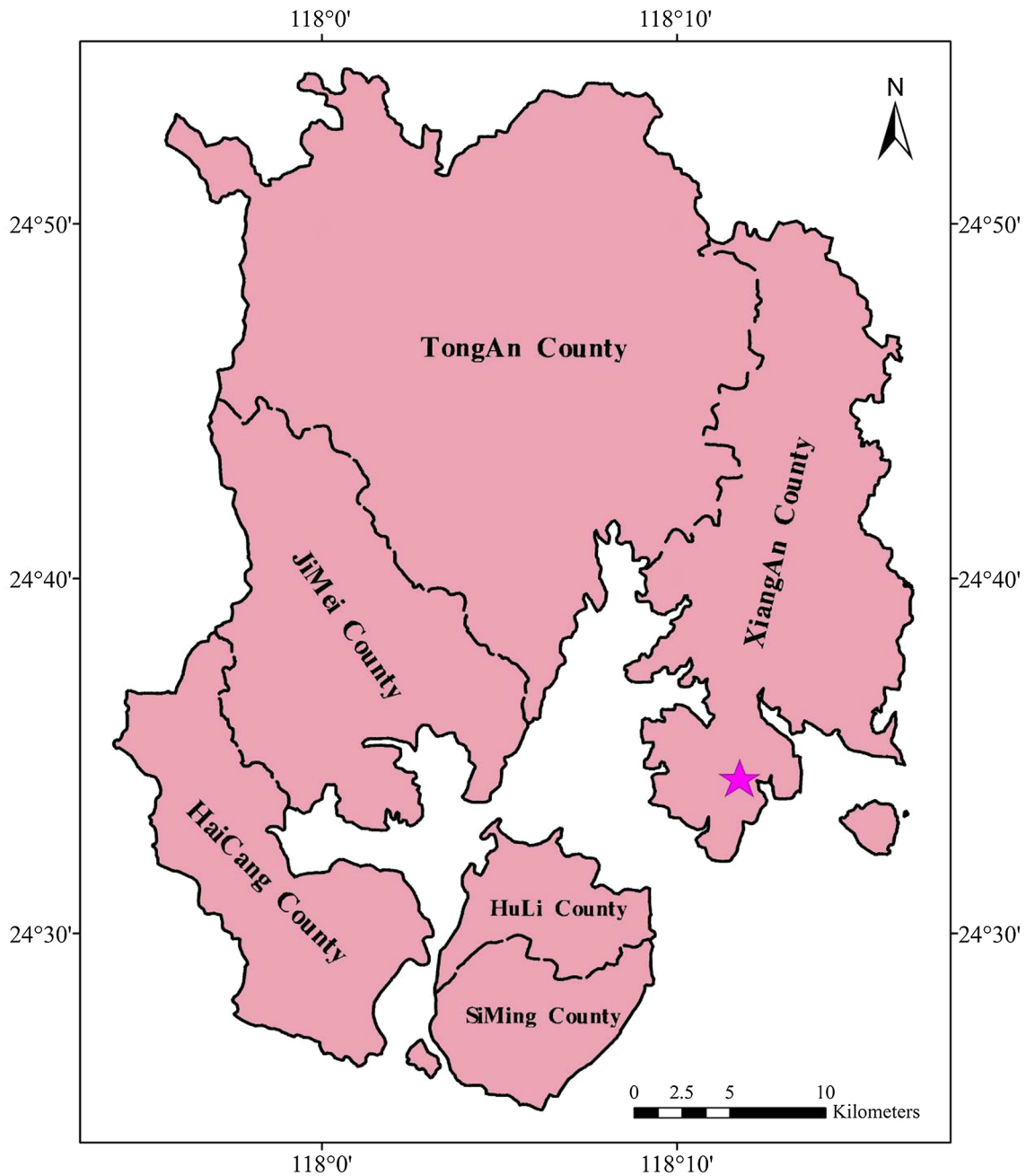


**Fig. 5** Location of the Dongshan geothermal field in Xiamen



clay and the inactive groundwater flow. The device measures the temperatures at the depths of 1 and 2 m and the in situ thermal conductivity for all the 18 measurement positions on November 14 and 15, 2014, when the climate was stable with the lowest rainfall in a year. Meanwhile, the altitude and geographical coordinates are recorded by GPS. Given that all measurements were completed within 2 days, the temperature variety caused by climate was negligible. Therefore, seasonal correction of the temperature data need not be conducted.



Fig. 6 Artesian spring in Dongshan geothermal field in 38.6 °C

## Results and discussion

### Temperature analysis and anomaly area identification

During temperature measurement, the probe should be inserted into the soil and the measurement should last 10 min for temperature equilibrium to avoid the influence of the disturbance caused by drilling. If the temperature sensor remains stable for at least 300 s, then the temperature is recorded for this position. The temperature nephogram for the Dongshan geothermal anomaly area is plotted by the method of interpolation shown in Fig. 8 according to the 2 m survey data.

Temperature data provided by the 2 m measurement allow the resolution of the potential geothermal area into two separate anomalies, namely a weak, narrow western anomaly with peak 2 m temperatures of 24–25 °C and a stronger, broad eastern anomaly with peak 2 m temperatures of 32–33 °C. Both of these anomalies are potentially significant. Boreholes 3 and 4 are located near the center of the western anomaly. Boreholes 10, 11, 12, 13, 14, 16, and 17 are located in the eastern anomaly. Boreholes 7, 8, and 9

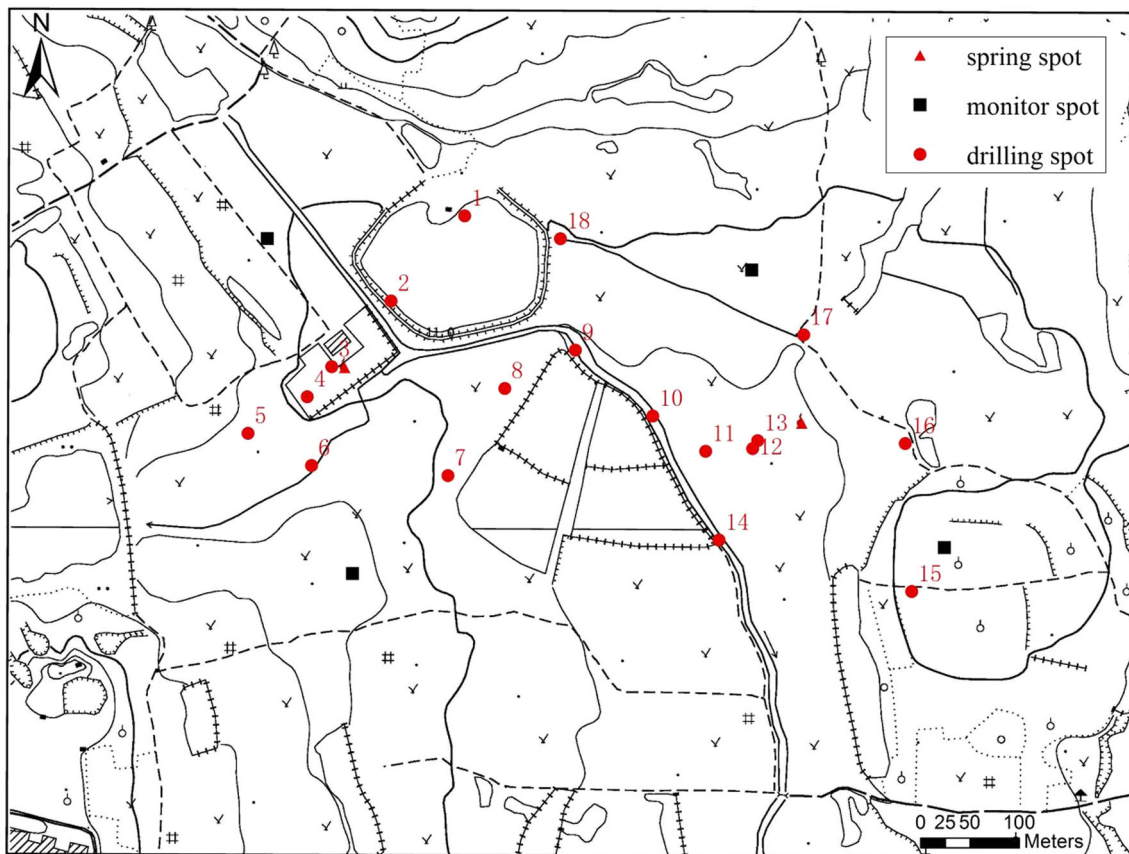
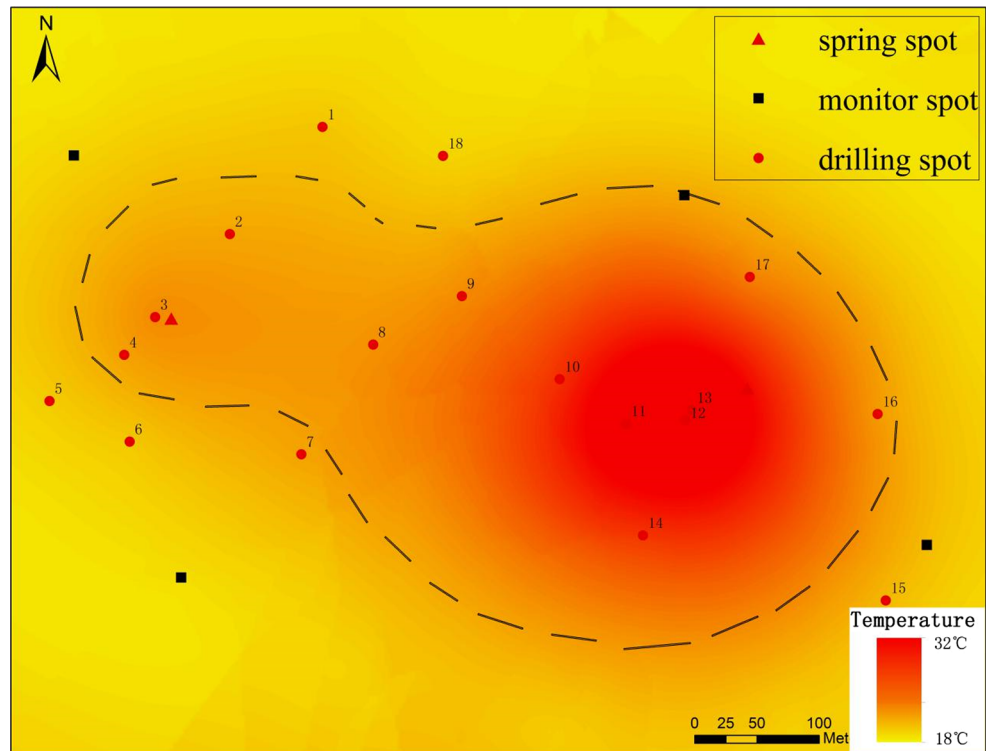


Fig. 7 Position of all 18 measurement boreholes

**Fig. 8** Temperature nephogram at 2 m depth of Dongshan geothermal field. The dotted-line region represents anomaly area



are located in the middle of the two anomaly centers. The other boreholes are outside the anomaly area. The maximum temperature difference can reach 13.5 °C among all 2 m boreholes. Correlations with the measurement wells show that 20 °C is the approximate threshold value above which temperatures clearly appear in relation to geothermal activity in the 2 m condition. Thus, the maximum anomaly temperature difference can be detected at 13 °C in the eastern area and 5 °C in the western area.

**Thermal conductivity and thermal flux analysis**

The water table and in situ thermal conductivity measured at the depths of 1 and 2 m are shown in Fig. 9. Several correlations show that increases in falling water tables decrease the thermal conductivity for both depths, and vice versa. When the water table is below 1 m, the 1 m thermal conductivity evidently declines; when the water table falls below 1.5 m, the 2 m thermal conductivity gradually declines. These results are consistent with the theoretical explanation that conducting conditions are poor because the soil pores are filled with air. Given that the thermal conductivity of water and air is 0.6 W/(m K) and 0.024 W/(m K) in the standard case (Yuan et al. 2010), respectively, replacing air with water decreases the thermal contact resistance because water forms an aqueous film between soil particles, thus increasing thermal conductivity.

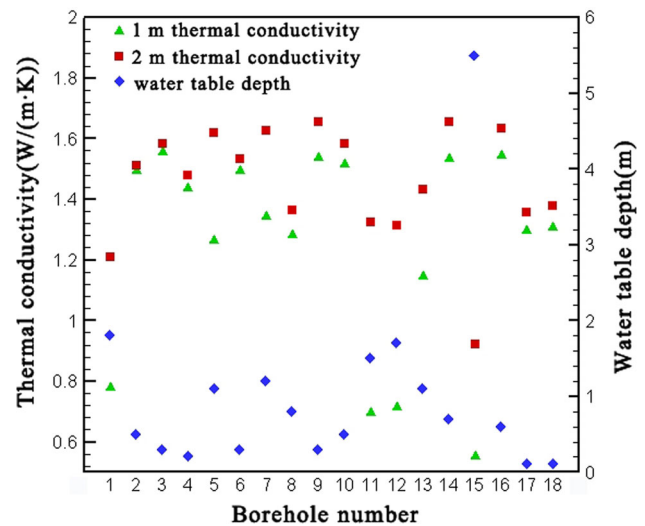
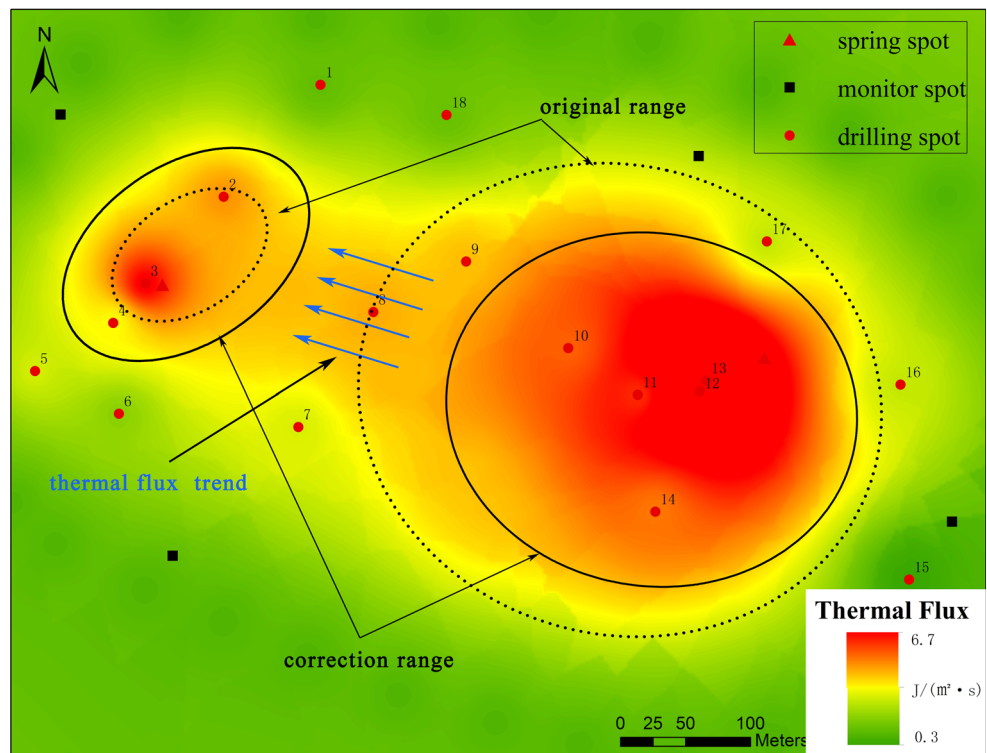


**Fig. 9** Scatter diagram of 1 m thermal conductivity, 2 m thermal conductivity, and water table

Divided by the water table, the underground soil can be simplified into the saturated soil layer and the unsaturated soil layer. Meanwhile, the two parts have different levels of thermal conductivity. Based on the drilling record during the measurement, water tables in all of the boreholes are less than 2 m, except for Borehole 15. The integrated thermal conductivity of the soil can be calculated by the average value of the 1 and 2 m thermal conductivity when the water table is less than 1 m. The interpolation method

**Fig. 10** Thermal flux nephogram at 2 m depth of Dongshan geothermal field. The original and correction-affected regions are shown. The transit tendency of the thermal flux is strong from east to west



is used to calculate the integrated thermal conductivity if the water table is deeper than 1 m but less than 2 m.

Using the temperature difference between 1 and 2 m depths as the temperature gradient, the shallow thermal flux can be calculated by the grid data of temperature and integrated thermal conductivity distribution. The shallow thermal flux nephogram is depicted in Fig. 10. The shallow thermal flux distribution basically matches the temperature nephogram that shows two geothermal flux peaks. The eastern peak is apparently larger than the western peak, and as the distance from the geothermal anomaly center increases, the thermal flux decreases. The thermal flux reflects the passing heat through the unit cross-sectional area by a unit of time. Compared with temperature distribution, analyses that combine thermal flux distribution will reveal more about the tendency of geothermal anomalies to vary. Thus, geothermal centers are more accurately depicted and survey accuracy is improved.

**Correction geothermal effect range**

Based on the temperature difference between anomaly threshold temperature and 2 m temperature, if the anomaly threshold temperature is defined in 20.0 °C (the average temperature of surface from previous monitoring data), then the anomaly range can be distinguished beyond a distance of 190 m (Fig. 11a) apart from the eastern anomaly center. However, only distance differentials of

70 m (Fig. 11a) can be distinguished from the western anomaly center.

Surface temperatures are easiest to measure and can be mapped in detail with thermal remote sensing. However, thermal remote sensing is strongly influenced by solar radiation, vegetation, and climate, which make it an unreliable stability criterion (Coolbaugh et al. 2007). However, the environmental influence decreases significantly in the 1 m depth temperature (Jia et al. 1986); thus, the correction geothermal affect range of the anomaly center is depicted by the difference between 2 m measure temperature and 2 m derivation temperature. The 2 m derivation temperature is calculated by 1 m temperature and in situ thermal conductivity. The correction geothermal affect range is distinguished in Fig. 11b. As the distance between anomaly center and borehole increases, the temperature difference decreases. Two correction affect regions are shown in the geothermal area, namely a broad eastern affect range with a conspicuous temperature difference in the radius of 150 m and a slightly smaller western affect range in the radius of 100 m. The original and correction affect regions are shown in Fig. 10. The correction affect regions perform better to reveal the real affect range to reduce the environment impact. Compared with the two correction regions, temperature variation is dramatic in the eastern area, which indicates that the intensity of the eastern anomaly is stronger than that of the western anomaly. Although the intensity of the eastern anomaly is evidently

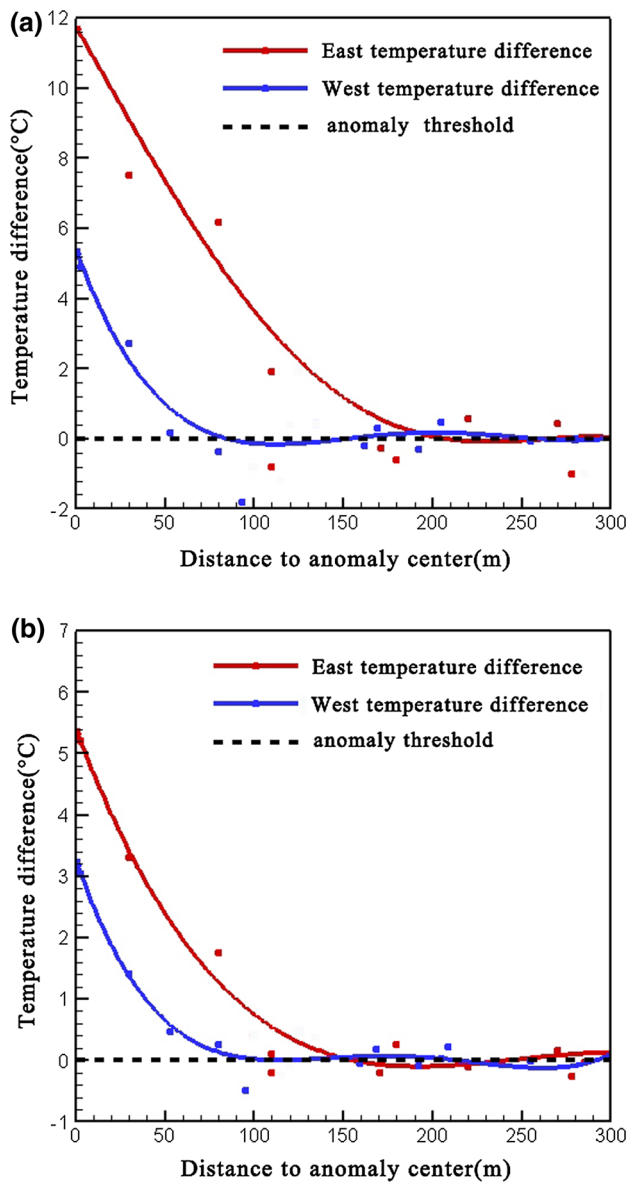


**Fig. 11** Temperature difference decreases as distance increases; when the temperature difference approaches 0 °C, the distance reflects the effect range. **a** Temperature difference between 2 m and anomaly threshold temperature. **b** Temperature difference between 2 m and 2 m derivation temperature

stronger than that of the western anomaly, the correction geothermal affect range of the eastern anomaly is just a little bigger than that of the western anomaly. This finding indicates that the geothermal anomaly center located in the western region is shallower than that in the eastern region.

### Surface and potential geothermal features

Figure 8 shows two thermal anomaly areas composed of an irregular oval shape with an east–west long axis. The temperature data of the 2 m depth are obtained from

Boreholes 8, 9, 10, and 11 between the eastern and western geothermal centers that are evidently affected by gradient changes. As the distance from the thermal flux peaks increased, the thermal flux decreased rapidly (Fig. 10). The decline rates in regions between two peaks were smaller, and the values of thermal flux were apparently higher than other parts, moving from east to west. Given the thermal flux flow trend and intensity in the anomaly area, a potential east–west stream of a high thermal flux strip is predicted to exist between the two geothermal centers. Although no direct geologic evidence could verify if this high thermal flux strip was formed by a fault, the following possibilities were considered: (1) A continuously gradient change in the thermal flux was visible between two thermal flux peaks without a low-value region. The thermal flux continuously changed, and a channel probably existed to transfer the thermal flux. (2) Based on survey data, chemical component of springs near both geothermal centers is broadly identical, indicating a potential hydraulic connection between the two geothermal centers. (3) Based on geologic data, a large NNW strike fault was discovered, and it passed through the western geothermal center. Under this indirect geologic background, the possibilities of a small fault between the two geothermal centers increased. Considering the given evidence, a potential fault is suspected across the two geothermal centers because the transit tendency of the thermal flux is strong from east to west. The potential fault plays a role in opening the flow channel, and the strike of the fault is consistent with the long axis of the geothermal anomaly area or high thermal flux strip. The temperature varied more apparently in the potential fault than in the surrounding area. Thus, an east–west striking fault with filled thermal fluids is predicted. Such a fault connects the two geothermal centers and affects thermal flux.

According to the previous survey data, spring artesian occurred in both the eastern and western anomaly areas with a temperature of approximately 40 °C. The flow rate in the western area was slightly larger than the flow rate in the eastern area. However, when several wells were drilled near the springs, the artesian phenomenon disappeared in the west spring and the flow rate increased significantly in the east spring. Therefore, the hydraulic connection really exists between the eastern and western areas and provides indirect evidence in support of the existence of a fault.

### The 20 m depth temperature inversion model forecast

Temperatures at depths >20 m are unaffected by the surface environment, and at these depths, recognizing and mapping a geothermal area becomes easier (LeSchack and Lewis 1983). Environmental influence evidently decreases

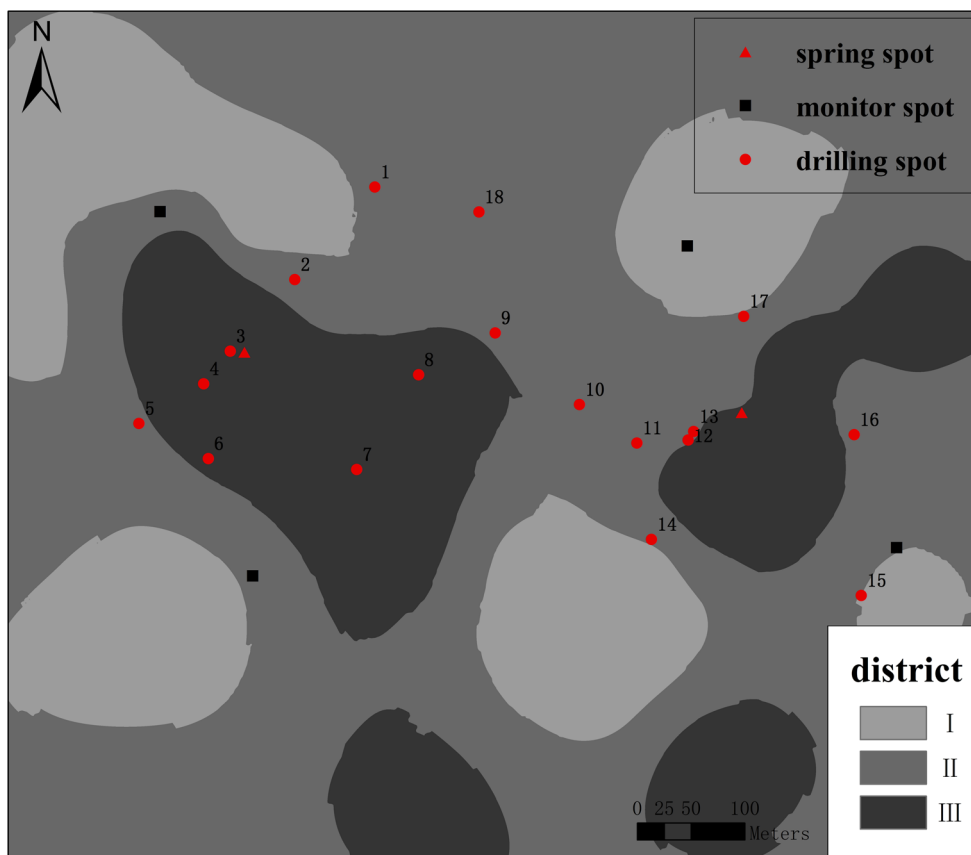
when the depth increases if the measurement is conducted below the depth of 1 m; thus, the underground temperature field deeper than 2 m can be approximately regarded as a steady temperature field. Based on this hypothesis, the underground temperature inversion model will be simplified as follows: (1) underground heat transfer occurs only as a form of heat conduction, ignoring heat convection and heat radiation; (2) the heat energy around the borehole transfers only along the drill direction, which belongs to a unidirectional heat conduction model; (3) throughout the process of heat conduction, the heat flow density from every layer is regarded as invariant or the lateral heat dissipation in each layer is ignored; (4) the thermal conductivity of every layer will not change with the variation in temperature or other factors. According to these simplified conditions, utilized the 2 m temperature data and integrated thermal conductivity, the 20 m temperature could be inverted by the Fourier Law.

The geothermal anomaly area is generally divided into three districts by stratum data shown in Fig. 12. In district I, the soil from the surface to 4 m in depth comprises clay, sandy clay, and silt; soil from 4 to 20 m is composed of sandy clay. In district II, soil at depths of 0–4 m comprises clay, sandy clay, and silt; soil from 4 to 16 m deep comprises sandy clay; and soil 16–20 m deep comprises

granite. In district III, soil from 0 to 4 m deep comprises clay, sandy clay, and silt; soil 4–10 m deep comprises sandy clay; and soil 10–20 m comprises granite. Except for Boreholes 3, 4, 6, 7, and 8, which are located in district III, all boreholes are located in district II. Based on the integrated thermal conductivity calculated by in situ measurement and laboratory tests, the 20 m temperature can be inverted using the steady-state heat conduction model (Fig. 13).

Figure 13a shows the real 20 m temperature isothermal line obtained by drilling wells, and Fig. 13b depicts the 20 m temperature isothermal line obtained by inversion temperature. The temperature distribution at a depth of 20 m is basically determined by comparing the inversion results. Two geothermal anomaly centers are clearly revealed among the geothermal anomaly area, and their intensity and location are basically consistent with the actual conditions provided by drilling data. According to the inversion data, the eastern geothermal center exhibited a temperature of 68.75 °C and the western geothermal center exhibited a temperature of 45.91 °C at a depth of 20 m. The average temperature error of all 18 boreholes at a 20 m depth is 3 °C, whereas the relative error between actual and forecast values is less than 10 %. The relationship between actual value and forecast value plotted

**Fig. 12** Stratigraphic regionalization of Dongshan geothermal field



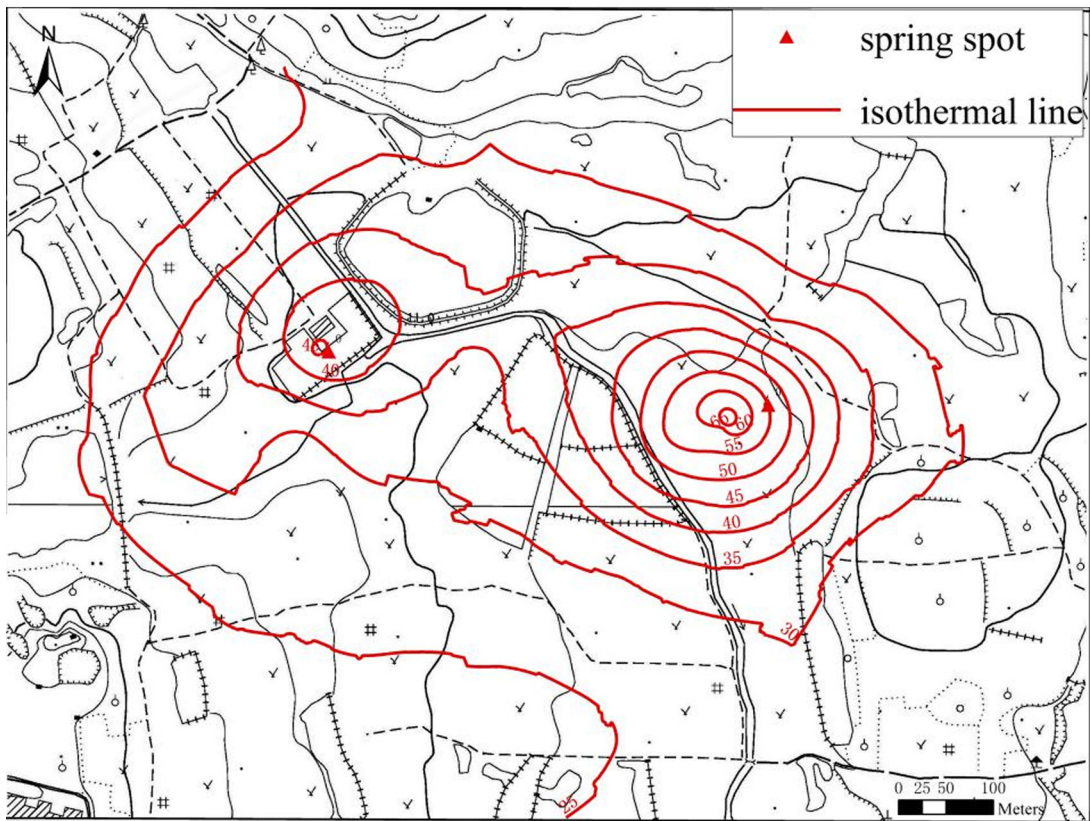
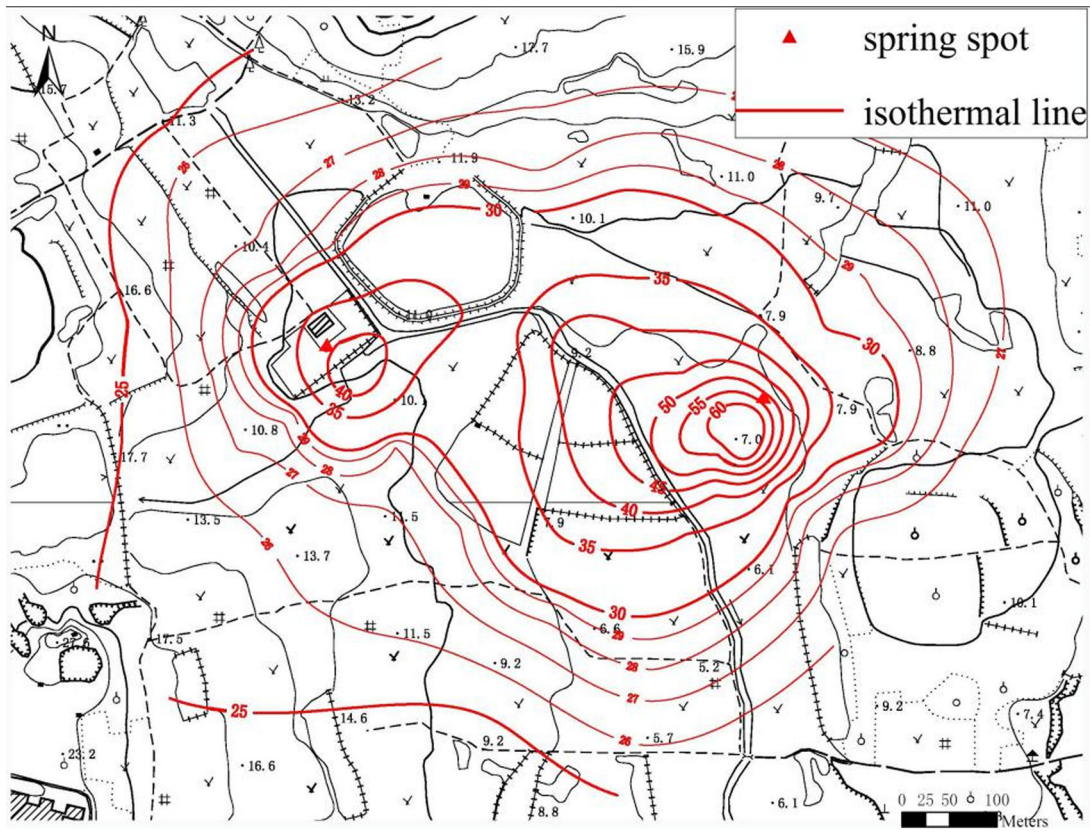


**Fig. 13** Isothermal line of Dongshan geothermal field at 20 m depth. **a** Isothermal line of Dongshan geothermal field at 20 m depth (described by drilling data). **b** Isothermal line of Dongshan geothermal field at 20 m depth (described by inversion temperature)

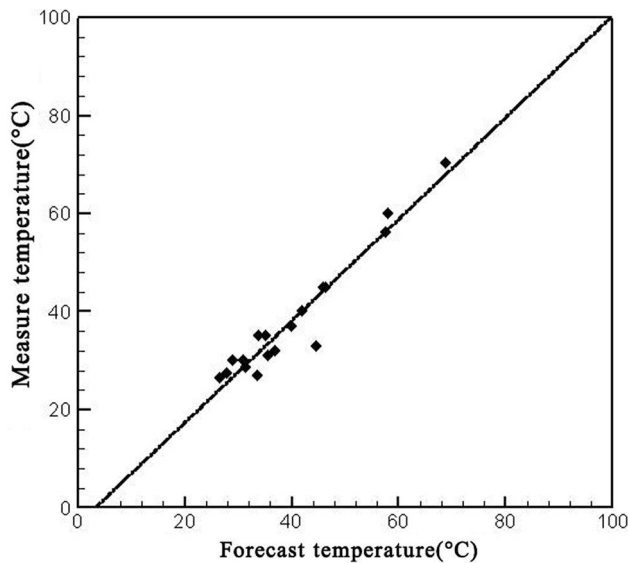


**Fig. 14** Correlation analysis between measured and forecast values of temperature

together is  $R^2 = 0.92859$  (Fig. 14). Although the forecast isothermal lines are generally slightly higher than the actual values, relatively high geothermal areas ( $>50\text{ }^\circ\text{C}$ ) are still well-reflected, which demonstrates an acceptable forecast result for underground temperature in limited 2 m survey data.

### Conclusion

An improved device for 2 m survey has been developed. It is calibrated by laboratory experiment. The entire setup weighs no more than 20 kg, is easy to assemble, is portable, and is suitable for a team of two or three individuals. The device adds in situ thermal conductivity measurement by the needle probe method based on original temperature measurements. The probe method has the advantages of small contact size and a short balancing time. Thus, temperature and thermal conductivity can be accurately measured by minimum impact in less than 10 min for every borehole. 2 m survey method and this improved device performed well in the Dongshan geothermal field. The survey accuracy has been proven by drilling wells. Based on the measured data, we achieved a small range of heat transfer calculation, shallow thermal flux calculation, and analysis of the relationship between temperature distribution and surface heat flux. Geothermal centers were located, and their anomaly

intensities were estimated. The 2 m survey result of the field experiment detected two geothermal anomaly centers, namely a strong one in the eastern region and a weak one in the western region. The geothermal affect range is corrected. The two centers achieve thermal contact by a potential fault. Based on the 2 m survey data, a steady-state heat conduction model was used to inverse the 20 m temperature. The forecast result shows that the eastern center exhibited a temperature of  $68.75\text{ }^\circ\text{C}$  and the western center exhibited a temperature of  $45.91\text{ }^\circ\text{C}$  at a 20 m depth.

The 2 m survey result of the field experiment in Dongshan geothermal field can be used to describe the geothermal anomaly in the area. Compared with the costly and time-consuming drilling survey during the preliminary stage of exploration, the 2 m survey with the improved device can provide reliable survey results. The successful identification of a potential geothermal anomaly area at Dongshan geothermal field demonstrates how 2 m temperature measurements can reduce the costs of geothermal exploration programs and increase their efficiency. Furthermore, they provide a greater likelihood of success in (1) locating thermal anomalies in the preliminary stage of exploration and (2) mapping hydrothermal-type geothermal resources in greater detail than normally possible with traditional survey devices. The comparison of actual values collected by drilling data with inverse forecast values demonstrates a strong correlation, which indicates that the 2 m survey is an effective initial geothermal survey method. Based on the 2 m survey results in the preliminary survey stage, temperature measurement wells can be more rationally sited in potential geothermal anomaly areas so that they can optimize drilling, reduce surveying length, and enhance returns in the subsequent stage.

**Acknowledgments** This study was supported by the National High Technology Research and Development Program of China (863 Program) (No. 2012AA052803), the Natural Science Foundation of China (Grant No. 41372239). Some of the data set has been provided by Geological Engineering Investigation Institute of Xiamen City.

### References

Aretouyap Z, Nouck PN, Nouayou R (2016) A discussion of major geophysical methods used for geothermal exploration in Africa. *Renew Sustain Energy Rev* 58:775–781

Carslaw HS, Jaeger JC (1959) *Conduction of heat in solids*. Clarendon Press, Oxford

Cartwright K (1974) Tracing shallow groundwater system by soil temperatures. *Water Resour Res* 10(4):847–855

Coolbaugh M, Sladek C, Faulds J, Zehner R, Oppliger G (2007) Use of rapid temperature measurements at a 2-meter depth to augment deeper temperature gradient drilling. In: *Thirty-second workshop on geothermal reservoir engineering*

Elachi C (1987) *Introduction to the physics and techniques of remote sensing*. Wiley, New York, p 413

- Jia L, Guan X, Xu J (1986) An investigation into some problems of one meter thermometry in geothermal exploration. *Geophys Geochem Explor* 10(2):115–122
- Kana JD, Djongyang N, Raïdandi D et al (2015) A review of geophysical methods for geothermal exploration. *Renew Sustain Energy Rev* 44:87–95
- Kappelmeyer O (1957) The use of near surface temperature measurements for discovering anomalies due to causes at depths. *Geophys Prospect* 5(3):239–258
- Kratt C, Sladek C, Coolbaugh MF (2010) Boom and bust with the latest 2 m temperature surveys: Dead Horse Wells, Hawthorne Army Depot, Terraced Hills and other areas in Nevada. *Geotherm Resour Counc Trans* 34:567–574
- LeSchack LA, Lewis JE (1983) Geothermal prospecting with Shallo-Temp surveys. *Geophysics* 48:975–996
- Manthena KC, Singh DN (2001) Measuring soil thermal resistivity in a geotechnical centrifuge. *Int J Phys Model Geotech* 1(4):29–34
- Olmsted FH (1977) Use of temperature surveys at a depth of 1 meter in geothermal exploration in Nevada. United States Geological Survey Professional Paper, 1044-B, 25
- Popov Y, Bayuk I, Parshin A (2012) New methods and instruments for determination of reservoir thermal properties. In: Proceedings, thirty-seventh workshop on geothermal reservoir engineering, Stanford University, Stanford, California
- Rao MV, Singh DN (1998) Laboratory measurement of soil thermal resistivity. *Geotech Eng Bull* 7(3):179–199
- Sladek C, Coolbaugh MF, Zehner RE (2007) Development of 2-meter soil temperature probes and results of temperature survey conducted at Desert Peak, Nevada, USA. *Geotherm Resour Counc Trans* 31:363–368
- Sugawa A (1961) The distribution of the 1 m-depth ground-temperature by the various heat source. *Geophys Bull Hokkaido Univ* 9:21–32
- Thompson GEK (1964) Proceedings of United Nations Conference on New Sources of Energy, vol 2, pp 386–401
- Trexler DT, Koenig BA, Ghusn G Jr, Flynn T, Bell EJ (1982a) Low-to-moderate-temperature geothermal resource assessment for Nevada: area specific studies, Pumpernickel Valley, Carlin and Moana. United States Department of Energy Geothermal Energy Report DOE/NV/10220-1 (DE82018598)
- Trexler DT, Koenig BA, Flynn T, Bruce JL, Ghusn G Jr (1982b) Low-to-moderate temperature geothermal resource assessment for Nevada: area specific studies, Final Report for the Period June 1, 1980–August 30, 1981: United States Department of Energy Geothermal Energy Report DOE/NV/10039-3 (DE81030487)
- Urakami K (1968) On a method of the underground temperature prospecting. *Geophys Bull Hokkaido Univ* 20:1–13
- Von Herzen V, Maxwell AE (1959) The measurement of thermal conductivity of deep-sea sediments by a needle-probe method. *J Geophys Res* 64(10):1557–1563
- Wang J, Hu S, Pang Z et al (2012) Estimate of geothermal resources potential for hot dry rock in the continental area of China. *Sci Technol Rev* 30(32):25–31
- Yuan XZ, Li N, Zhao XY et al (2010) Study of thermal conductivity model for unsaturated unfrozen and frozen soils. *Rock Soil Mech* 31(9):2089–2694
- Zehner RE, Tullar KN, Rutledge E (2012) Effectiveness of 2-meter and geoprobe shallow temperature surveys in early stage geothermal exploration. *Geotherm Resour Counc Trans* 36:835–842
- Zhang YJ, Yu ZW, Huang R et al (2009) Measurement of thermal conductivity and temperature effect of geotechnical material. *Chin J Geotech Eng* 31(2):213–217